Electronic Supplementary Information

Bicomponent blend-directed amplification of alkyl chain effect on the 2D structures

Yoshihiro Kikkawa,*[,1] Manami Ishitsuka,[2] Ayumi Kashiwada,[2]

Seiji Tsuzuki,[1] and Kazuhisa Hiratani [1]

[1] National Institute of Advanced Industrial Science and Technology (AIST), Tsukuba Central 4, 1-1-1 Higashi, Tsukuba, Ibaraki 305-8562, Japan

[2] Department of Applied Molecular Chemistry, College of Industrial Technology, Nihon University, 1-2-1 Izumi-cho, Narashino, Chiba 275-8575, Japan

1. Experimental detail

1-1. Synthesis and Characterization

1-2. STM Observation

2. Enlarged and additional STM images

2-1. STM images of OC_n and CC_n

2-2. STM images of blends with different ratio

2-3. Wide-area STM images of blends

2-4. Effect of solute concentration on the blending

2-5. Heterogeneous blends

2-6. Plausible molecular models of OC_n and CC_n

2-7. In situ STM imaging of OC_{15} and the blend with CC_{15}

2-8. In situ blending of CC_{16} and OC_{16}

3. Discussion on the hydrogen bonds and FT-IR spectra

1. Experimental Detail

1-1. Synthesis and Characterization

The reagents and solvents used in this study were purchased from Kanto, Tokyo Chemical Industry, or Wako Pure Chemical Industry, and used without further purification. All the compounds were characterized by using ^{1}H NMR (Bruker Avance 500 spectrometer), FT-IR (JASCO FT/IR420) using a thin film method on a KBr plate, and elemental analysis (CE Instruments EA1110).

All of the isobutenyl ether compounds possessing alkyl tails were prepared as follows: synthesis of **OC$_n$** (Fig. S1(A)) was performed as reported previously.[S1] Briefly, the isobutenyl naphthoeic acid chloride **1** (0.5 mmol) was dissolved in tetrahydrofuran (THF), and alkyl alcohol (1 mmol) and triethylamine (2 mmol) was added and reacted for 1 day. In the case of **CC$_n$** (Fig. S1(B)), a solution of isobutenyl binaphthylamine **2** (0.5 mmol) in 5 ml THF with triethylamine (2 mmol) was added to alkyl acid chloride (1 mmol), and the solution was stirred at 60 ˚C for 3 hours. Then, the solvent was evaporated under reduced pressure, and they were purified by a silica gel column chromatography with chloroform as an eluent.

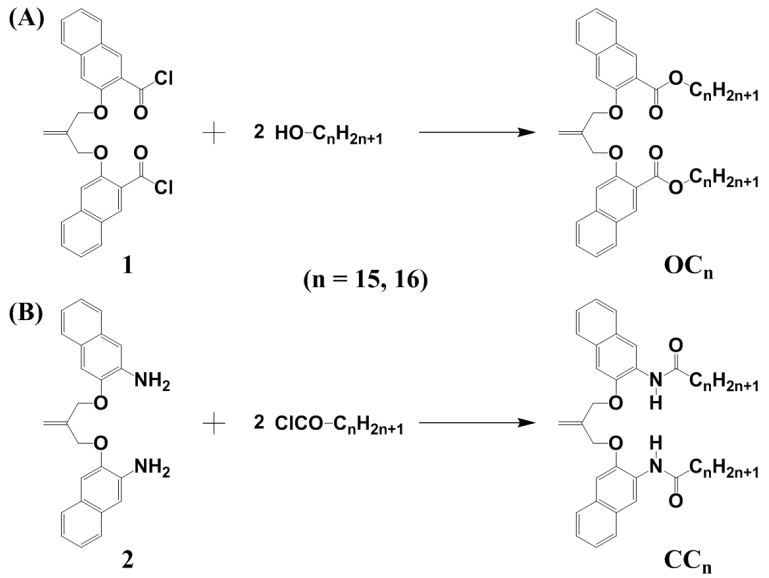

Fig. S1 Synthetic procedure and chemical structures of isobutenyl ether compounds, in which the alkyl chains are connected with ester (**OC$_n$**: (A)) and carbamoyl (**CC$_n$**: (B)) groups (n = 15 and 16).

OC_{15}: ^{1}H NMR ($CDCl_3$): δ = 0.88 (t, *J* = 7.5 Hz, 6H, CH_3), 1.24 (broad, 44H, CH_2), 1.39 (4H, m, CH_2), 1.74 (m, 4H, CH_2), 4.31 (t, *J* = 6.9 Hz, 4H, O-CH_2), 4.91 (s, 4H, =C-CH_2-O), 5.59 (s, 2H, CH_2=C), 7.28 (s, 2H, Naph-H), 7.37 (dd, *J* =7.5 7.5 Hz, 2H, Naph-H), 7.48 (dd, *J* = 7.5 7.5 Hz, 2H, Naph-H), 7.69 (d, *J* = 8.2 Hz, 2H, Naph-H), 7.82 (d, *J* = 8.1 Hz, 2H, Naph-H), 8.29 (s, 2H, Naph-H), IR (KBr): 745(Naph), 1071(C-O-C), 1632(C=C), 1731(C=O) cm^{-1}, Anal. Calcd for $C_{56}H_{80}O_6$・1/2 H_2O: C, 78.37; H, 9.51. Found: C, 78.44; H, 9.37.

OC_{16}: ^{1}H NMR ($CDCl_3$): δ = 0.88 (t, *J* = 6.4 Hz, 6H, CH_3), 1.24 (broad, 48H, CH_2), 1.37 (4H, m, CH_2), 1.73(m, 4H, CH_2), 4.31 (t, *J* = 6.6 Hz, 4H, O-CH_2), 4.91 (s, 4H, =C-CH_2-O), 5.58 (s, 2H, CH_2=C), 7.28 (s, 2H, Naph-H), 7.37 (dd, *J* =6.8 6.8 Hz, 2H, Naph-H), 7.48 (dd, *J* = 7.8 7.8 Hz, 2H, Naph-H), 7.69 (d, *J* = 8.2 Hz, 2H, Naph-H), 7.82 (d, *J* = 7.6 Hz, 2H, Naph-H), 8.29 (s, 2H, Naph-H), IR (KBr): 743(Naph), 1066(C-O-C), 1630(C=C), 1720(C=O) cm^{-1}, Anal. Calcd for $C_{58}H_{84}O_6$・1/2 H_2O: C, 78.60; H, 9.67. Found: C, 78.64; H, 9.45.

CC_{15} : ^{1}H NMR ($CDCl_3$): δ = 0.88 (t, *J* = 7.0 Hz, 6H, CH_3), 1.25 (broad, 48H, CH_2), 1.63 (m, 4H, CH_2), 2.24 (t, *J* = 7.6 Hz, 4H, O-CH_2), 4.91 (s, 4H, =C-CH_2-O), 5.58 (s, 2H, CH_2=C), 7.18 (s, 2H, Naph-H), 7.35 (d, 2H, *J* = 6.3 Hz, Naph-H), 7.36 (d, 2H, *J* = 6.1 Hz, Naph-H), 7.59 (dd, 4H, *J* = 6.1 6.1 Hz, Naph-H), 7.77 (dd, 4H, J = 6.2 6.2 Hz, Naph-H), 7.91 (s, 2H, N-H), 8.89(s, 2H, Naph-H), IR (KBr): 741(Naph), 1179(C-O-C), 1632(C=C), 1665(C=O), 3322(N-H) cm^{-1}, Anal. Calcd for $C_{56}H_{82}N_2O_4$・1/4 H_2O: C, 78.97; H, 9.76; N, 3.29. Found: C, 78.95; H, 9.71; N, 3.23.

CC_{16}: ^{1}H NMR ($CDCl_3$): δ = 0.88 (t, *J* = 6.9 Hz, 6H, CH_3), 1.25 (broad, 52H, CH_2), 1.62 (m, 4H, CH_2), 2.24 (t, *J* = 7.6 Hz, 4H, O-CH_2), 4.91 (s, 4H, =C-CH_2-O), 5.58 (s, 2H, CH_2=C), 7.18(s, 2H, Naph-H), 7.35(d, 2H, *J* = 6.0 Hz, Naph-H), 7.36(d, 2H, *J* = 6.4 Hz, Naph-H), 7.59 (dd, 4H, *J* = 6.2 6.2 Hz, Naph-H), 7.77 (dd, 4H, *J* = 6.2 6.2 Hz, Naph-H), 7.91 (s, 2H, N-H), 8.89 (s, 2H, Naph-H), IR (KBr): 741(Naph), 1179(C-O-C), 1632(C=C), 1665(C=O),

3322(N-H) cm^{-1}, Anal. Calcd for $C_{58}H_{86}N_2O_4 \cdot 1/4\ H_2O$: C, 79.18; H, 9.91; N, 3.18. Found: C, 79.24; H, 9.88; N, 3.06.

1-2. STM Observation

Low-current mode STM (Veeco Instruments, CA: Nanoscope IIIa multimode SPM) operation was performed to record the 2D structural features of isobutenyl compounds in a molecular level. Mechanical cut Pt/Ir (90 : 10) wire was used as STM tips. Basically, the **OC$_n$** and **CC$_n$** were independently dissolved in 1-phenyloctane at the concentration of 0.2 mM. An aliquot of the compounds in 1-phenyloctane was deposited onto the fleshly cleaved HOPG (ZYB grade, NT-MDT, Russia), and the STM observations were carried out at the HOPG/solvent interface. The reproducibility of STM images was secured by repeating the STM observations several times with different tips and samples. The underlying HOPG lattice was applied as an internal standard to correct the STM images by using SPIP software (Image Metrology, Denmark). In addition, the solute concentration effect on the 2D structure formation was studied in the range of 0.01–0.4 mM.

Both ex situ and in situ blending of **OC$_n$** and **CC$_n$** were separately carried out. The ex situ experiment was performed by pre-mixing the **OC$_n$** and **CC$_n$** with different ratio and concentrations before the STM studies. In the case of in situ experiment, the **CC$_n$** in 1-phenyloctane was added to the already-existing drop of the **OC$_n$** on the HOPG, and vice versa. The experimental conditions are indicated on each figure caption.

S1 K. Omori, Y. Kikkawa, M. Kanesato, K. Hiratani, *Chem. Lett.* **2010**, *39*, 1039.

2. Additional STM images

2-1. STM images of OC_n and CC_n

STM observations were performed for **OC_n** and **CC_n** (n = 15 and 16) at HOPG/1-phenyloctane interface. Fig. 2S shows the STM images of **OC_n** and **CC_n** with different alkyl chain length. Regardless of the alkyl chain length, the **OC_n** showed dumbbell shaped structures, whereas linear structures were formed for **CC_n**. Effect of solute concentration on the 2D structure formation was studied for **OC_n** and **CC_n**. The dumbbell shaped structures for **OC_n** were formed in the concentration range from 0.01–0.5 mM. In the case of **CC_n**, linear structures could be imaged by STM in the range of 0.05–0.5 mM, whereas stable 2D structures were not formed at the solute concentration below 0.05 mM.

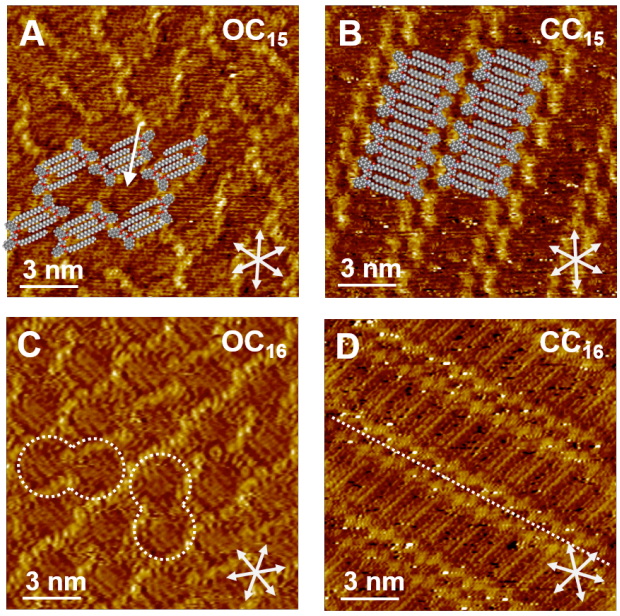

Fig. S2 STM images of **OC_n** and **CC_n** physisorbed at the HOPG/1-phenyloctane interface and tentative molecular models superimposed on the STM images. The 2D structural feature is depicted in the dashed line (C and D). The vacant space indicated by an arrow in (A) can be filled with solvent molecule of 1-phenyloctane.[S2] Panels (A) and (B) are corresponding to Fig. 2 in the main text. Tunneling conditions: (A) **OC_{15}**, I = 2.2 pA, V = -620 mV; (B) **CC_{15}**, I = 1.5 pA, V = -530 mV; (C) **OC_{16}**, I = 2.0 pA, V = -880 mV; (D) **CC_{16}**, I = 2.8 pA, V = -600 mV. Lattice constants: (A) a = 3.4 ± 0.1 nm, b = 12.0 ± 0.1 nm, γ = 66 ± 1 °; (B) a = 1.9 ± 0.1 nm, b = 3.9 ± 0.1 nm, γ = 89 ± 1 °; (C) a = 3.2 ± 0.1 nm, b = 12.4 ± 0.1 nm, γ = 68 ± 5 °; (D) a = 1.9 ± 0.1 nm, b = 4.1 ± 0.1 nm, γ = 85 ± 2 °.

2-2. STM images of blends with different ratio

The 0.2 mM solutions of $\mathbf{OC_n}$ and $\mathbf{CC_n}$ in 1-phenyloctane were blended ex situ with different ratio, and STM observations were performed, as shown in Figs, S3 and S4. Depending on the alkyl chain length and blend ratio, various 2D structures were formed such as star-like ($\mathbf{OC_{15}} \geq \mathbf{CC_{15}}$), lozenge-shaped ($\mathbf{OC_{15}} < \mathbf{CC_{15}}$), twist-like ($\mathbf{OC_{16}} > \mathbf{CC_{16}}$), and linear structures ($\mathbf{OC_{16}} \leq \mathbf{CC_{16}}$).

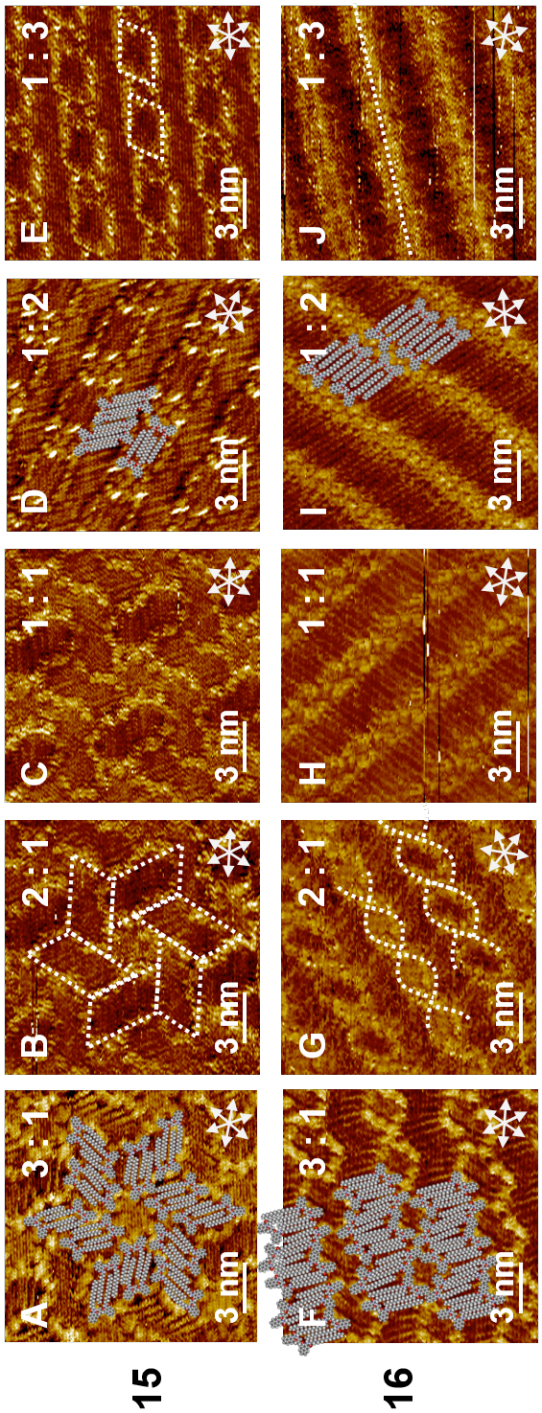

Fig. S3 STM images of $\mathbf{OC_n}$ and $\mathbf{CC_n}$ blends with different ratio. The blend ratio is shown in the right corner of each STM image in the order of $\mathbf{OC_n}$: $\mathbf{CC_n}$. The 2D structural feature is depicted in the dashed line as star-like (*St*; B), lozenge-shaped (*Lo*; E), twist-like (*Tw*; G), and linear structure (*Li*; J). The carbon numbers of the blend system are 15 (A–E) and 16 (F–J), respectively. Plausible molecular models are superimposed on STM images. Panels (A), (E), (F) and (J) are corresponding to Fig. 3 in the main text. Tunneling conditions: (A) I = 1.5 pA, V = -200 mV; (B) I = 2.0 pA, V = -540 mV; (C) I = 2.5 pA, V = -400 mV; (D) I = 2.0 pA, V = -630 mV; (E) I = 2.0 pA, V = -300 mV; (F) I = 1.4 pA, V = -660 mV; (G) I = 3.4 pA, V = -380 mV; (H) I = 1.8 pA, V = -940 mV; (I) I = 1.8 pA, V = -630 mV; (J) I = 2.0 pA, V = -660 mV.

The repeating units of each unique structure in $\mathbf{OC_n}$ and $\mathbf{CC_n}$ blends were defined, as shown in Fig. S3-2. The measurements of the unit cell parameters were performed for star-like ($\mathbf{OC_{15}}$: $\mathbf{CC_{15}}$ = 3 : 1), lozenge-shaped ($\mathbf{OC_{15}}$: $\mathbf{CC_{15}}$ = 1 : 3), twist-like ($\mathbf{OC_{16}}$: $\mathbf{CC_{16}}$ = 3 : 1), and linear structures ($\mathbf{OC_{16}} \leq \mathbf{CC_{16}}$ = 1 : 3), and they are listed in Table S1.

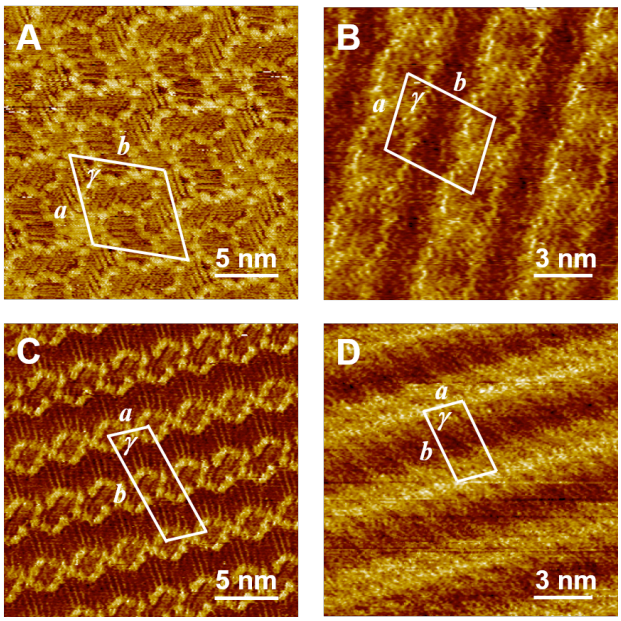

Fig. S3-2 STM images of $\mathbf{OC_n}$ and $\mathbf{CC_n}$ blends, in which the repeating units of each unique structure were defined: (A) star-like ($\mathbf{OC_{15}}$: $\mathbf{CC_{15}}$ = 3 : 1); (B) lozenge-shaped ($\mathbf{OC_{15}}$: $\mathbf{CC_{15}}$ = 1 : 3); (C) twist-like ($\mathbf{OC_{16}}$: $\mathbf{CC_{16}}$ = 3 : 1); (D) linear structures ($\mathbf{OC_{16}}$: $\mathbf{CC_{16}}$ = 1 : 3).

Table S1 Unit cell parameters measured from the STM images in Fig. S3-2.

	Blend ratio $\mathbf{OC_n}$: $\mathbf{CC_n}$	*a* (nm)	*b* (nm)	*γ* (deg)
star-like structure (n = 15)	3 : 1	7.3 ± 0.3	7.7 ± 0.1	65 ± 1
lozenge-shaped structure (n = 15)	1 : 3	4.2 ± 0.2	7.9 ± 0.3	79 ± 4
twist-like structure (n = 16)	3 : 1	3.4 ± 0.2	10.0 ± 0.3	77 ± 3
linear structure (n = 16)	1 : 3	1.9 ± 0.2	4.2 ± 0.2	81 ± 2

2-3. Wide-area STM images of blends

The blend ratio affected the 2D phase structures. At the ratio of **OCn** : **CCn** = 1 : 1.5, both lozenge-shaped and star-like structures were observed as phase-separation, whereas linear and twist-like morphologies were formed at the **OCn** : **CCn** = 1.5 : 1.

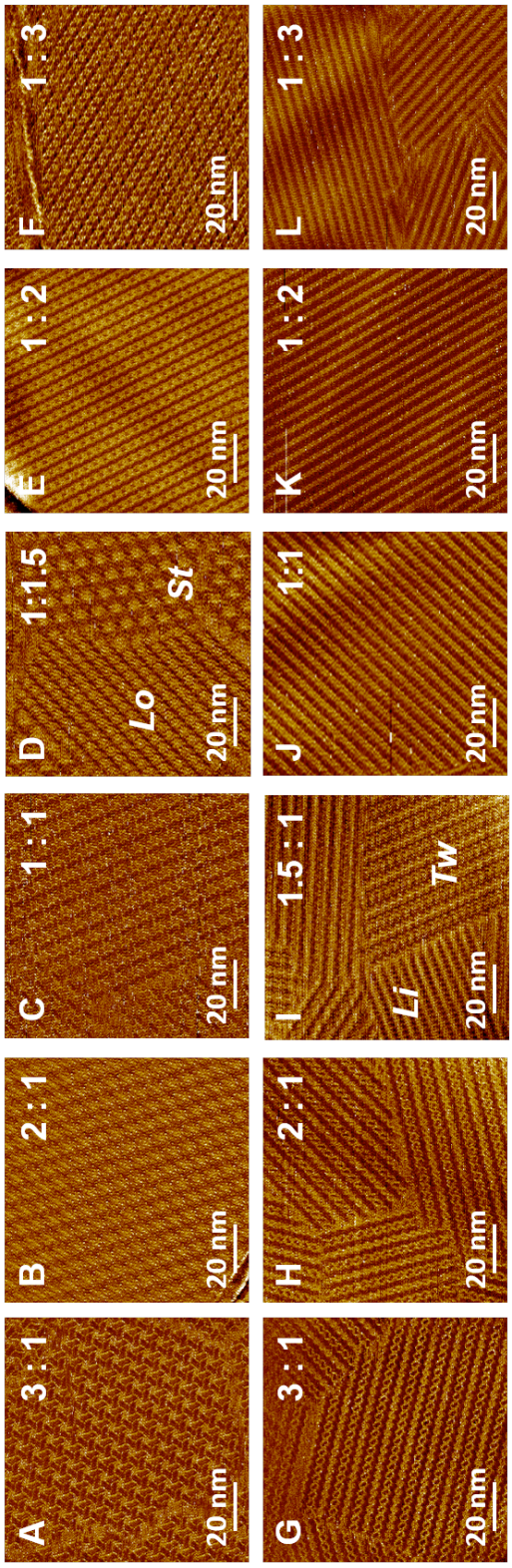

Fig. S4 Wide area STM images of $\mathbf{OC_n}$ and $\mathbf{CC_n}$ blends with different ratio. The blend ratio is shown in the right corner of each STM image in the order of $\mathbf{OC_n}$: $\mathbf{CC_n}$. The carbon numbers of the blend system are 15 (A–F) and 16 (G–L), respectively. Tunneling conditions: (A) I = 2.0 pA, V = -200 mV; (B) I = 1.8 pA, V = -540 mV; (C) I = 2.5 pA, V = -400 mV; (D) I = 2.0 pA, V = -350 mV; (E) I = 1.8 pA, V = -600 mV; (F) I = 2.0 pA, V = -100 mV; (G) I = 1.6 pA, V = -630 mV; (H) I = 2.5 pA, V = -620 mV; (I) I = 2.0 pA, V = -300 mV; (J) I = 2.0 pA, V = -940 mV; (K) I = 1.7 pA, V = -1000 mV; (L) I = 2.0 pA, V = -680 mV.

2-4. Effect of solute concentration on the blending

Since the concentration dependent polymorphism is sometimes observed at the solid/liquid interface,[S2] effect of the solute concentration on the 2D structure formation was studied in the bicomponent blend system. Within the range of 0.01–0.4 mM, there was no concentration effect on the 2D structure changes, and the 2D structural features were the same as Fig. 2 (0.2 mM), despite the fact that the concentration of each component altered after the blending as shown in Table S2. In addition, 2D structural alteration was not found only in the components of $\mathbf{OC_n}$ and $\mathbf{CC_n}$, as shown in the section 2-1. These results suggest that the present 2D structural change after the bicomponent blend is not derived from the solute concentration effect, but from supramolecular interactions of the components.

Table S2 Concentrations of each component after the blending and total solute concentration.

Total solute concentration (mM)	Blend ratio (OC_n : CC_n)			
	3:1		1:3	
	OC_n	**CC_n**	**OC_n**	**CC_n**
0.4	0.3	0.1	0.1	0.3
0.2	0.15	0.05	0.05	0.15
0.05	0.0325	0.0125	0.0125	0.0325

S2 For example: S. Lei, K. Tahara, F. C. De Schryver, M. Van der Auweraer, Y. Tobe, S. De Feyter, *Angew. Chem. Int. Ed.* **2008**, *47*, 2964.

2-5. Heterogeneous blends

Blending of $\mathbf{OC_{15}}$ with $\mathbf{CC_{16}}$ and $\mathbf{OC_{16}}$ with $\mathbf{CC_{15}}$ was carried out, and STM images are shown in Fig. S5. The total solute concentration was fixed to 0.2 mM. The $\mathbf{OC_{15}} > \mathbf{CC_{16}}$ and $\mathbf{OC_{15}} < \mathbf{CC_{16}}$ blends revealed the linear structures, which had been found in the $\mathbf{OC_{16}} \leq \mathbf{CC_{16}}$ blends. In contrast, $\mathbf{OC_{16}} > \mathbf{CC_{15}}$ and $\mathbf{OC_{16}} < \mathbf{CC_{15}}$ blends displayed the star-shaped structures, which had been formed in the $\mathbf{OC_{15}} > \mathbf{CC_{15}}$ blends. Therefore, it seems that $\mathbf{CC_n}$ compounds dominate the formation of 2D structures. Note that blending of $\mathbf{OC_{15}}$ with $\mathbf{OC_{16}}$ and $\mathbf{CC_{15}}$ with $\mathbf{CC_{16}}$ resulted in the formation of original dumbbell shaped ($\mathbf{OC_n}$) and linear structures ($\mathbf{CC_n}$), and that the blending of identical components didn't provide the structural changes. If the structural formation in the blend system is based on the intermolecular hydrogen bond only, the structural features should be the same as homogeneous blends of $\mathbf{OC_n}$ with $\mathbf{CC_n}$ (n = same). This result suggests that the alkyl chain length plays a definitive role for the unique 2D structure formation, especially for the twisted and lozenge shaped structures.

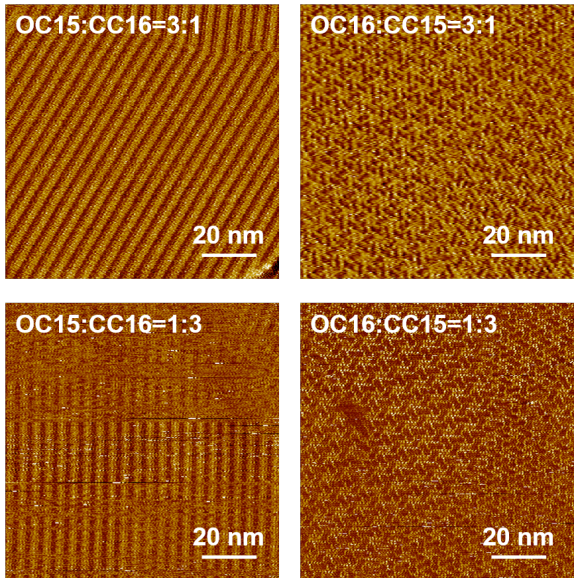

Fig. S5 STM images of heterogeneous blends at HOPG/1-phenyloctane interface.

2-6. Plausible molecular models of OC_n and CC_n

Assuming the plane fit of the molecules on the HOPG surface, stable molecular configurations of basic skeleton of **OC_n** and **CC_n** without long alkyl tails (**OC*** and **CC***) were calculated on the basis of the DFT method (B3LYP/6-311G** level). In both cases, the parallel conformation of naphthalene unit is more stable compared to the flipped one, as shown in Fig. S6. Especially for the **CC***, the configuration seemed to be stabilized by the five-membered intramolecular hydrogen bonds between the ether oxygen and –NH in the carbamoyl linkage. Since the alkyl chains were connected with naphthalene unit through ester- and carbamoyl linkage, orientation of the naphthalene unit decides the direction of alkyl tails. On the basis of the present DFT calculation, stable conformations of **OC*** and **CC*** was applied for the molecular models proposed for the STM images in the single component as well as bicomponent system.

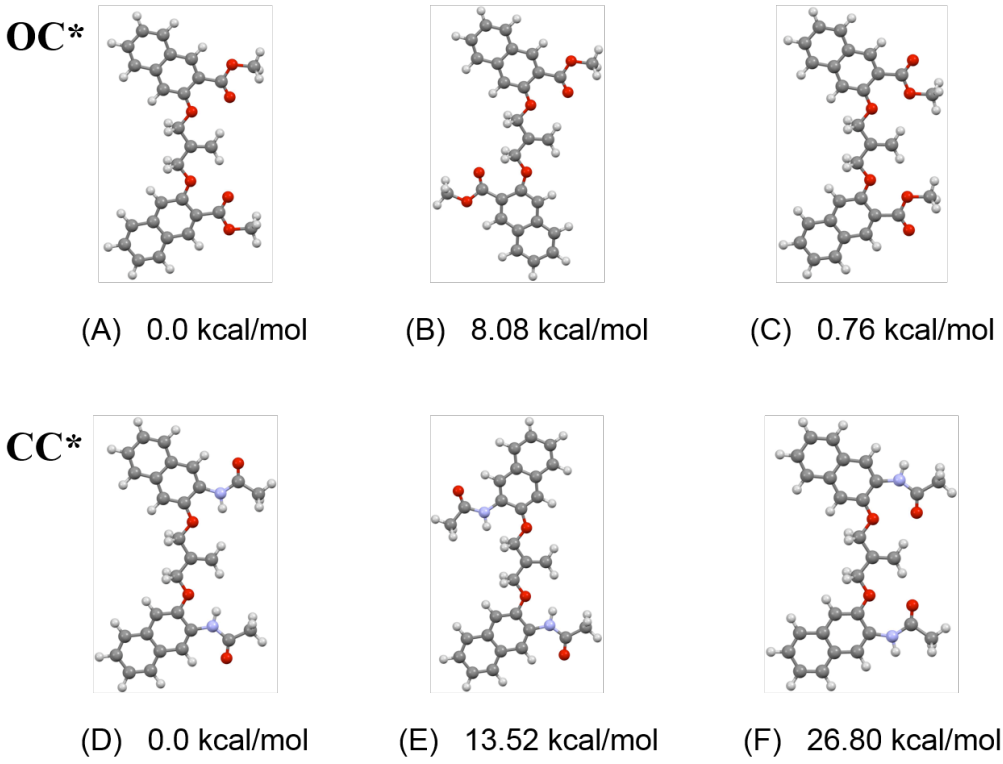

Fig. S6 Stable molecular configurations of **OC*** and **CC***, in which the long alkyl tails of **OC_n** and **CC_n** are replaced to methyl groups. (A-C): **OC***, (D-E): **CC*.** The values under the molecular model are relative energies for **OC*** and **CC***.

2-7. In situ STM imaging of OC_{15} and the blend with CC_{15}

For the in situ blend experiment, 2D pattern of **OC_{15}** was formed on the HOPG (Fig. S7(A)), and an aliquot of **CC_{15}** was added to the already-existing drop of the **OC_{15}** on the HOPG (Fig. S7(B)), resulting in the structural change from dumbbell to star shapes. Further addition of **CC_{15}** solution allowed to follow the gradual structural change by STM (Fig. S7(C)-(F)).

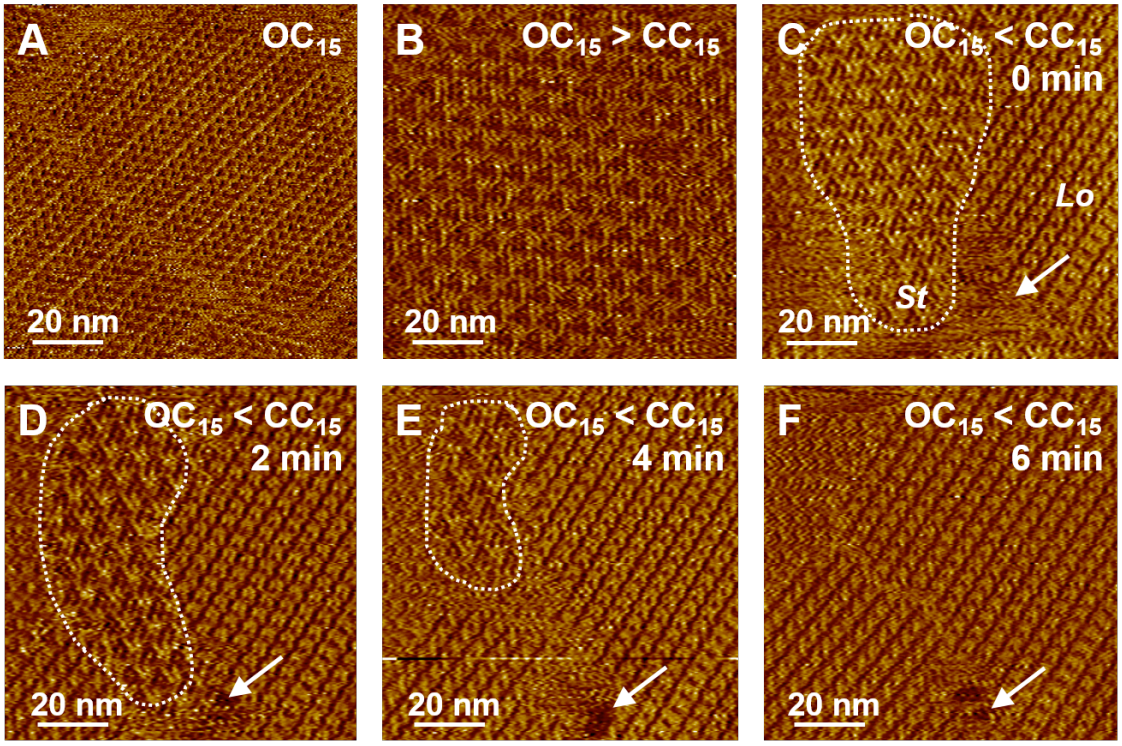

Fig. S7 STM image of **OC_{15}** physisorbed at the HOPG/PO interface (A), and in situ blending of **OC_{15}** with **CC_{15}** (B–F). In (B), the **CC_{15}** solution was added into the already-existing drop of **OC_{15}** on the HOPG surface to be the blend ratio of **OC_{15}** > **CC_{15}** (B). Then, further addition of **CC_{15}** solution to be **OC_{15}** < **CC_{15}** allowed to follow the time-dependent 2D structural change by the STM, and the capture time after the blending is indicated at the right corner of each STM image (C–F). The domain size of star-like structure (*St*) circled by a dashed line gradually diminished, whereas the lozenge shaped structures (*Lo*) increased. The arrow in (C–F) indicates the same position during the STM imaging. In this figure, panels (B), (C), (E) and (F) are shown as Fig. 4 in the main text. Tunneling conditions: (A) I = 2.0 pA, V = -280 mV; (B) I = 1.5 pA, V = -150 mV; (C–F) I = 2.0 pA, V = -280 mV.

2-8. In situ blending of CC_{16} and OC_{16}

Linear structure of **CC_{16}** was formed in Fig. S8(A), and addition of **OC_{16}** solution resulted in the structural change to twist-like morphology (Fig. S8(B)-(D)).

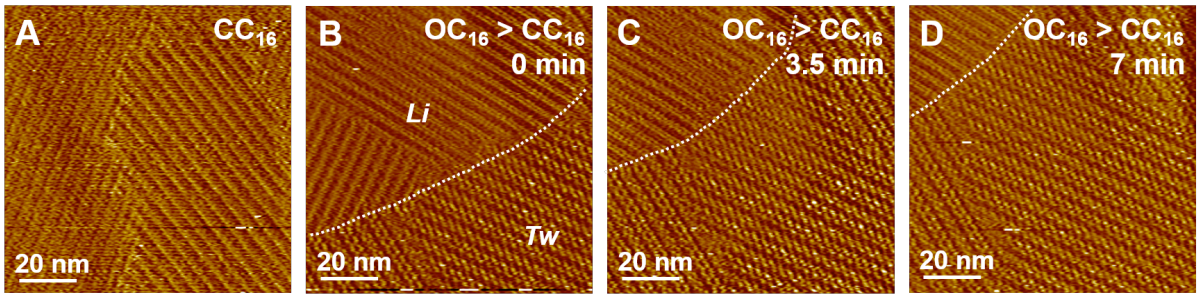

Fig. S8 STM images of **CC_{16}** (A) and following in situ blending with **OC_{16}** at the ratio of **OC_{16}** > **CC_{16}** (B–D). In (B), excess amount of **OC_{16}** was added to the already-existing drop of **CC_{16}** on the HOPG, and gradual structural change was followed by STM (C and D). Tunneling conditions: (A) I = 2.0 pA, V = -710 mV; (B–D) I = 2.0 pA, V = -590 mV.

3. Discussion on the hydrogen bonds and FT-IR spectra

To study the origin of the unique 2D structures formation after the blending, it is important to check whether the hydrogen bond between -C=O in **OC_n** and -N-H in **CC_n** exist or not. Then, FT-IR experiment was tried for the bulk sample, although the STM experiments were performed at solid/liquid interface. Fig. S9 shows the FTIR of **OC_n**, **CC_n** and their blends at the ratio of **OC_n** : **CC_n** = 1 : 1. There was no peak shift of -N-H stretch (3322 cm^{-1}) before and after the blending, suggesting that new intermolecular hydrogen bond is not formed after the bicomponent blend.

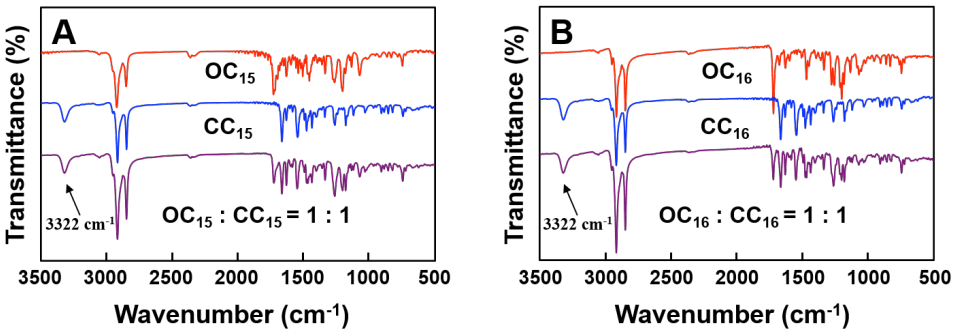

Fig. S9 FT-IR spectra of **OC_n**, **CC_n** and their blends at the ratio of **OC_n** : **CC_n** = 1 : 1. (A) n = 15; (B) n = 16. The peak position of 3322 cm^{-1} (-N-H stretch) remained unchanged after the

blending, suggesting that hydrogen bond is not newly formed between the **OC$_n$** and **CC$_n$** in the bulk.

Recent high level ab initio calculations revealed that stabilization energy of all-trans n-hexane dimer in all-trans conformation is 2.51 kcal/mol in coplanar orientation, in which the symmetry planes of two n-hexanes are coplanar.[S2] In the present study, pentadecyl (C15) and hexadecyl (C16) chains are connected to the isobutenyl ether core part through ester and carbamoyl linkage. Therefore, the stabilization energy of C15 and C16 is calculated as:

C15) 2.51 kcal/mol ÷ 6 × 15 = 6.27 kcal/mol

C16) 2.51 kcal/mol ÷ 6 × 16 = 6.69 kcal/mol

In addition, there is adsorption energy of alkyl chains onto HOPG, which is reported as 64 meV per methylene group.[S3] The adsorption energy is calculated as:

C15) 64 meV × 23.1 × 15 = 22.2 kcal/mol

C16) 64 meV × 23.1 × 16 = 23.7 kcal/mol

Then, total stabilization energy of the self-assembled compounds can be at least ca. 30 kcal/mol. Taking the general hydrogen bonding energy (4–6 kcal/mol)[S4] into account, the formation of new intermolecular hydrogen bonds will not play dominant roles in stabilizing the unique 2D structures in the present blending system. As shown in the DFT calculation in section 2.6, the conformation of **CC$_n$** is already stabilized by the five-membered intramolecular hydrogen bonds between the ether oxygen and –NH in the carbamoyl linkage. If the intermolecular hydrogen bond between -C=O in **OC$_n$** and -N-H in **CC$_n$** is newly formed after the blending, the intramolecular hydrogen bond in **CC$_n$** must be once broken and followed by the intermolecular hydrogen formation. To form the intermolecular hydrogen bonds, -C=O in **OC$_n$** and -N-H in **CC$_n$** should be faced with each other, and therefore the plausible molecular structures of **OC$_n$** and **CC$_n$** are the conformations (C) and (F) shown in Fig. S6, respectively. The relative energy of the conformation (C) of **OC$_n$** compared to the

most stable conformation is only 0.76 kcal/mol. However, the relative energy of conformation (F) of $\mathbf{CC_n}$ compared with the most stable one is 26.8 kcal/mol, which cannot be compensated by the formation of intermolecular hydrogen bond, which is generally 4–6 kcal/mol. The FT-IR spectra and energetic considerations suggest that the dominant interaction for the formation of unique 2D structures after the blending is van der Waals interaction between the alkyl chain units in $\mathbf{OC_n}$ and $\mathbf{CC_n}$.

S2 S. Tsuzuki, K. Honda, T. Uchimaru, M. Mikami, *J. Phys. Chem. A*. **2004**, *108*, 10311.

S3 A. J. Gellman, K. R. Paserba, *J. Phys. Chem. A*. **2002**, *106*, 13231.

S4 M. –H. Hao, *J. Chem. Theory Comput.* **2006**, *2*, 863.